Hindawi
Advances in Materials Science and Engineering
Volume 2019, Article ID 4219323, 11 pages
https://doi.org/10.1155/2019/4219323

Research Article

Experimental Investigations on Aircraft Blade Cooling Holes and CFD Fluid Analysis in Electrochemical Machining

Mingxia Chai, Zhiyong Li, Hongjuan Yan, and Xiaoyu Sun

School of Mechanical Engineering, Shandong University of Technology, 255049 Zibo, China

Correspondence should be addressed to Zhiyong Li; lzy761012@sdut.edu.cn

Received 11 June 2019; Revised 17 July 2019; Accepted 28 July 2019; Published 28 August 2019

Academic Editor: Frederic Dumur

The flow field distribution in an interelectrode gap is one of the important factors that affect the machining accuracy and surface quality in the electrochemical machining (ECM) process for aircraft blades. In the ECM process, some process parameters, e.g., machining clearance, processing voltage, and solution concentration, may result in electrolyte fluid field to be complex and unstable, which makes it very difficult to predict and control the machining accuracy of ECM. Therefore, 30 sets of experiments for cooling hole making in ECM were carried out, and furthermore, the machining accuracy and stability of cooling hole were concentrated. In addition, the flow channel of the geometrical model of the gap flow field was established and analyzed according to the electrolyte flow state simulation by CFD. The effects of the flow velocity mode on the machining accuracy and stability for cooling hole making were investigated and determined in detail.

1. Introduction

With the development of aviation technology, modern aircraft engines can generate higher power for the same unit size and therefore improve fuel efficiency. Turbine blades possess a large number of cooling channel holes (as shown in Figure 1), and the typical cooling hole diameter and aspect ratio are in the range of 1–4 mm and 40–200, respectively. Generally speaking, turbine blades are made of super-heat-resistant alloys, such as nickel alloy and titanium alloy. Peetermans and Lehmann [1] stressed that turbine blades are made of single-crystal nickel-based superalloys that can withstand the highest temperatures and loads. Liu et al. [2] pointed out that although the military and civil high bypass pressure ratio turbofan engines has adopted the existing mature materials and technologies, it still has special requirements in the manufacture of some key parts, which need to be tackled. Bilgi et al. [3] explained that it is difficult for conventional hole making processes to drill these holes in nickel-based superalloys due to their low thermal conductivity, high toughness, high work hardening, and special aspect ratios. Fortunately, the emergence of nontraditional machining has effectively solved the above problems. They are (i) electrical discharge machining (EDM), (ii) laser beam machining (LBM), and (iii) electrochemical machining (ECM). Research works by Liu et al. [4] showed that traditional nanosecond laser drilling is a high-efficiency and low-cost manufacturing process for hole making, but unavoidable recasting layer or even microcracks may appear on the machined surface due to laser heat transfer. Wang [5] pointed out that the EDM can achieve high perforation speed and machining efficiency and also can easily produce the recasting layer. Zhang et al. [6] in their work indicated that electrochemical drilling is an important method for producing small holes in difficult-to-machine materials such as titanium alloy and nickel-based alloy. A study by Jain and Pandey showed that the accuracy of holes could greatly be improved by use of bits rather than bare tools as ECM tools, and they found that the overcut difference between the top and bottom of the drilled hole is less than 5 mm [7]. On the shop floor, the use of bit can be used to drilling holes. Ali et al. [8] conducted a partial design experiment with STEM to study the effects of important process parameters on hole diameter and hole taper, provided the guidelines for selecting process conditions, and developed the process model of selecting the process parameters for a desired hole

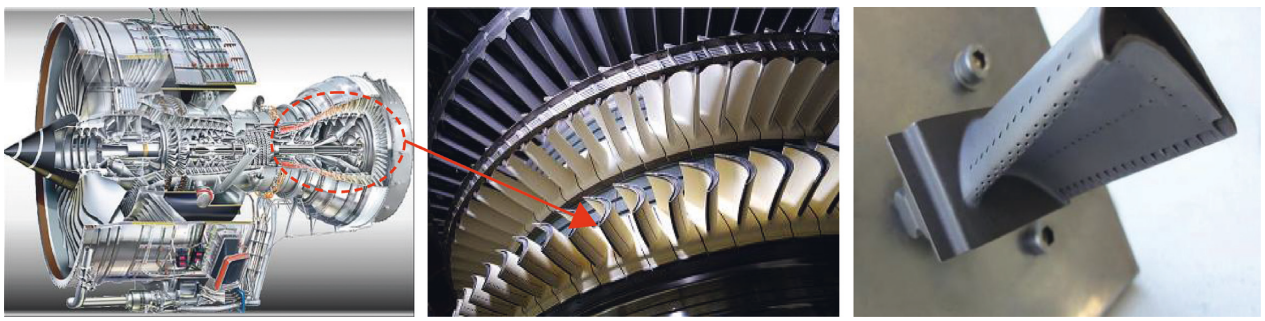

(a) (b) (c)

Figure 1: (a) Aircraft engine and (c) cooling holes on (b) the turbine blade's surface.

quality. This provides a basis for the parameter selection of the electrochemical machining hole. Chen et al. [9] conducted orthogonal experiments to investigate ECM of Ti60 to determine the influences of some electrochemical process parameters on the surface roughness. They found that using suitably optimized parameters for ECM can greatly decrease the surface roughness of a workpiece. And the optimization parameters have been successfully applied in blisk blades. Wang et al. [10] used wedge-shaped electrodes in the STEM process to machine an inclined cooling hole and obtained high-quality holes with large inclination angles. Li et al. [11] used vacuum extraction shaped tube electrolytic machining (VE-STEM) to manufacture cooling holes of Inconel 718. In their study, the effects of key process parameters, i.e., applied voltage, electrolyte concentration, and tool feed rate, on process efficiency, form accuracy, and process stability has been investigated. The effect size was determined using an ANOVA analysis. From the results of the electrochemical drilling process using the regression analysis, ANOVA, and Taguchi technique, Rao et al. [12] completed the optimization of machining parameters and established a radial overcut model. By using this model and referring to the optimization parameters, the quality of the holes in the actual production can be improved. Gao et al. [13] managed to eliminate the blackened layer by traditional wire electrochemical micromachining (WEEM) of type 304 stainless steel through using the double-pulsed WEMM method. Rajurkar et al. [14] pointed out that ECM is widely used in turbine blade making because it has no tool electrode loss, no residual stresses on the machined surface, and comparable high material removal rate. However, improving the machining accuracy and processing stability of ECM has been proved to be a challenging task because the physical features (e.g., electrolytic products and electrolyte flow field) in ECM area are hard to control during the process.

As the electrolyte flows through the gap in the ECM process, the metal workpiece material is dissolved and produces electrolytic products constantly, which are discharged by the circulation of the electrolyte flow. Therefore, the discharge velocity of the electrolytic products is determined by the distribution of the electrolyte flow velocity and velocity field mode, which affects the manufacturing efficiency of the cooling hole. In addition, the electrolytic products, which were not discharged in time and stranded in the electrolyte flow passage, may usually result in the electrolyte flow field disorder and eddy appearance. The eddy can further reduce the update speed of the electrolyte in the ECM gap. With the continuous process of ECM, the workpiece material dissolution is slower and slower in eddy area, and the machining efficiency of ECM is reduced. In addition, short circuit burns and serious electrolyte flow marks can appear together, which affect the machining accuracy and stability seriously. Recently, with the rapid developments of the computational fluid dynamics (CFD), some numerical simulations were concentrated on the machining accuracy and process stability of hole making in ECM. Bilgi et al. [15] used the STEM process with pulsed power supply to investigate the manufacturing process of Ni-based alloy deep holes and optimize the process parameters. Based on the theory of ECM gap distribution, Bilgi et al. [16] established a prediction model for the machining gap in ECM of tube electrodes and got more accurate results than anyone else had done before. The proposed model helps in determining the side gap current during electrochemical drilling and would help in evaluating the depth-averaged radial overcut. Hu et al. [17] managed to decrease the stray corrosion in trepanning ECM through using forward flow of compressed air to blow into the cathode to form a gas film on the machined surface and carried out the numerical simulations of the distributions of compressed air and electrolytes in the machining area. In their research, the gas film layer could reduce stray corrosion and taper angle and improve the machining surface quality and accuracy of the workpiece. Wu et al. [18] used CFD to simulate the eddy distribution in cavity electrolysis process, obtained the eddy status and pressure distribution in the ECM gap, and then guided the optimization design of tool cathode. Zhu et al. [19] put forward a new dynamic lateral flow mode and verified its rationality through simulation by using computational fluid dynamics software and experiment. However, the main goals of the above research relative to CFD of flow field in ECM are how to improve the design accuracy of tool cathode and optimize the process parameters. The CFD simulations for the electrolyte flow velocity field mode are relatively scarce. The studies on the effects of the electrolyte flow velocity field mode on machining efficiency in ECM are also still less.

This paper mainly studied the influences of ECM parameters (applied voltage U and electrolyte concentration ξ) on the machining accuracy, stability, and efficiency in

aircraft cooling hole making by the STEM process. The modes of the electrolyte flow field were determined by CFD. Moreover, the effects of the electrolyte flow field mode on EMC efficiency were analyzed based on CFD computing results in detail.

2. Experimental Setup and STEM Process

Considering the characteristics of STEM, the experimental setup shown in Figure 2 is selected. It is composed of a control system based on the PC movement platform, tool cathode feed system, electrolyte supply system, and monitoring system. The control system can control the multiaxis position and motion speed of the machine tool and display the relevant parameters when the machine tool moves in real time. The tool feed system adopts a servodrive and realizes the closed-loop control of feed through the grating ruler with the resolution of 1 μm. In the utilization of the electrolyte supply system, the electrolyte is ejected from the end face outlet of the tube electrode by using the high-pressure pump pipe and flows back to the electrolyte tank after impacting the machining area. The monitoring system is used to inspect the variation of machining current in STEM for cooling hole making.

Figure 3 is the schematic diagram of STEM for aeroengine cooling hole making. STEM is an electrochemical process to remove metal by anodic dissolution in an electrolytic cell in which the workpiece is anode and the tool is the cathode. The two electrodes are immersed in the electrolyte solution. The electrolyte flows out of the tube electrode inner hole, takes away the dissolved products and heat, and finally completes the cooling hole making.

Two independent process parameters were selected to conduct the parametric study, i.e., applied voltage (U) and electrolyte concentration (ξ). All other machining parameters in STEM for cooling hole making were constant. In all experiments, inlet electrolyte pressure P_{inlet} was 0.6 MPa, outlet electrolyte pressure P_{outlet} 0.1 MPa, and tool cathode feed rate f was 0.48 mm/min. Figure 3 is the schematic diagram of STEM for aeroengine cooling hole making. The tool electrode is a brass tube electrode with a diameter of 0.8 mm and an inner diameter of 0.3 mm. Its cylindrical surface is insulated by epoxy with a thickness of 50 μm in the radial direction, and 0.2 mm length is left without insulation at the end of the tube electrode. The workpiece is made of high-temperature nickel-based alloy and Inconel 718 sheet with a thickness of 1.7 mm, and its chemical composition is shown in Table 1. Since most of the cooling holes in the turbine blades are inclined from 15° to 60° to blades surface, all cooling holes machined in experiments are inclined in 45° to the Inconel 718 sheet normal direction in this study. As a result, the depths of cooling holes are 2.4 mm.

In order to verify the effects of ECM process parameters on machining accuracy and machining efficiency, the unilateral side gap (Δs) and machining removal rate (MRR) are used as the evaluation indexes of machining accuracy and machining efficiency, respectively.

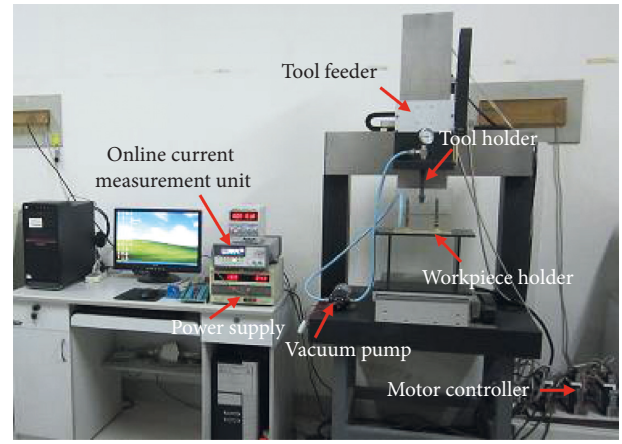

Figure 2: Experimental setup of the STEM process.

Δs refers to the distance between the side wall of the tube electrode and the inner wall of the cooling hole when the ECM equilibrium state is achieved. Due to its inability to measure online during processing, it is generally measured after ECM process. The calculation formula is as follows:

$$\Delta s = \frac{D - d}{2}, \tag{1}$$

where D is the diameter of the cooling holes (μm) and d is the diameter of the tube electrode (μm).

MRR is another important parameter to evaluate the efficiency of cooling hole making. It is the weight difference per unit time of the workpiece before and after ECM, and its calculation formula is as follows:

$$\text{MRR} = \frac{M - m}{\rho \cdot T}, \tag{2}$$

where M is the initial weight of workpiece before ECM process (g), m is the weight of workpiece after ECM process (g), ρ is the density of Inconel 718 (8.24 g/mm^3), and T is the ECM time (min).

3. Experiment Works

3.1. Design of Experiments. In the STEM process, applied voltage is a key process parameter, which can not only establish the electric field between the electrochemical machining electrodes and ensure the continuous process of electrochemical machining but also maintain the current density during the machining process. In addition, the function of an electrolyte is to build the electrochemical reaction electrode system and take away electrolyte products and heat in time. Therefore, its composition and concentration are also the vital factors in the ECM process. Thus in this study, two independently controllable parameters selected to conduct the parametric study of STEM were applied voltage (U) and electrolyte concentration (ξ). Electrolyte composition is $NaNO_3$ solution. Many typical process experiments on optimization of ECM parameters have been completed by researchers and scholars, which provide good references for the selection of experimental

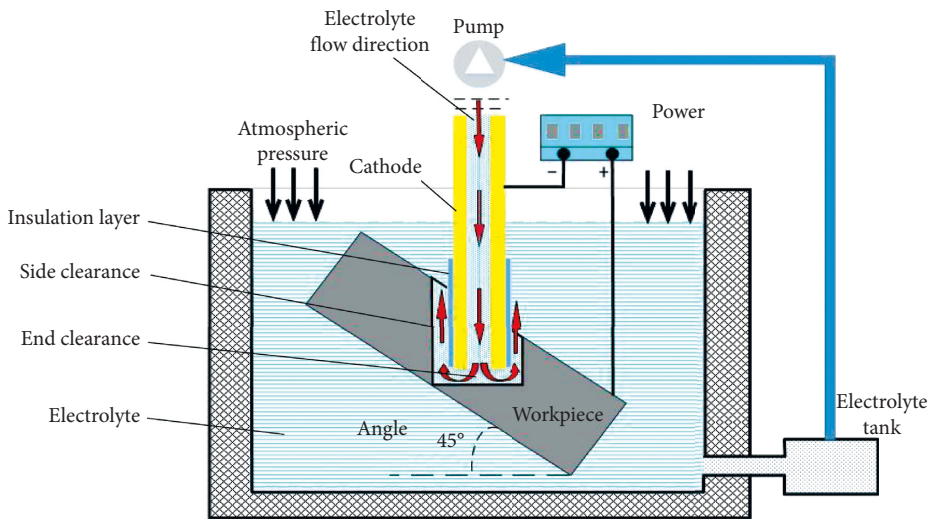

Figure 3: The schematic diagram of shaped tube electrochemical machining (STEM).

Table 1: Chemical compositions of Inconel 718.

Element	C	Al	Ti	Cr	Fe	Ni	Nb	Mo
(wt.%)	3.12	0.44	0.86	13.91	16.13	38.84	4.24	2.67

parameters in this experiment. Wang et al. [20] machined stainless steel of 0Cr18Ni9 with vacuum extraction of electrolytes in $NaNO_3$ solution. They found the machining process was not carried out when the tool feed rate is over 15 μm/s at the applied voltage of 15 V. Zhu et al. [21] proposed a new method of making multiple holes with electrolyte-extraction supply. Based on this method, holes in the stainless steel plate with a thickness of 2 mm were machined successfully with an applied voltage of 10 V and 180 g/L $NaNO_3$ aqueous solution during the experiments. Under the processing condition of $NaNO_3$ (electrolyte concentration 15%, inlet pressure 0.55 MPa, and applied voltage 20 V), Wei et al. [22] obtained the wheel hub holes with high accuracy. Based on the above references and actual ECM process requirements, the full factorial design of experiments was conducted in this experiment, and the parameter selection is shown in Table 2.

3.2. Effects of Applied Voltage on Machining Accuracy and Efficiency. As listed in Table 2, the values of the applied voltage used in cooling hole making are determined to be 5, 7, 9, 11, and 13 V, and the tool electrode feed rate is 0.48 mm/min. Figures 4 and 5 describe the variation curves of the unilateral side gap Δs and MRR with the applied voltage U.

In Figure 4, the unilateral side gap Δs increases with increasing of applied voltage at all six certain electrolyte concentrations. For example, at the electrolyte concentration of 15% (the other ECM process conditions are unchanged), the unilateral side gap Δs increases by more than 126.2% (from 108.5 μm to 245.5 μm) as the applied voltage increases from 5 V to 13 V. The possible reasons for the unilateral side gap Δs increase with increased applied voltage U could be attributed to the fact that as the applied voltage increases, the current density between tube tool and cooling hole becomes higher, which in turn leads to more workpiece material dissolution per unit time, and then the larger unilateral side gap. The same variation tendency between MRR and applied voltage can be observed in Figure 5. MRR increases with the increase of applied voltage when the electrolyte

Table 2: ECM experiment conditions.

Number	Voltage (V)	Concentration (wt.%)	Feed rate (mm/min)
1	5	5	0.48
2	5	7	0.48
3	5	9	0.48
4	5	11	0.48
5	5	13	0.48
6	5	15	0.48
7	7	5	0.48
8	7	7	0.48
9	7	9	0.48
10	7	11	0.48
11	7	13	0.48
12	7	15	0.48
13	9	5	0.48
14	9	7	0.48
15	9	9	0.48
16	9	11	0.48
17	9	13	0.48
18	9	15	0.48
19	11	5	0.48
20	11	7	0.48
21	11	9	0.48
22	11	11	0.48
23	11	13	0.48
24	11	15	0.48
25	13	5	0.48
26	13	7	0.48
27	13	9	0.48
28	13	11	0.48
29	13	13	0.48
30	13	15	0.48

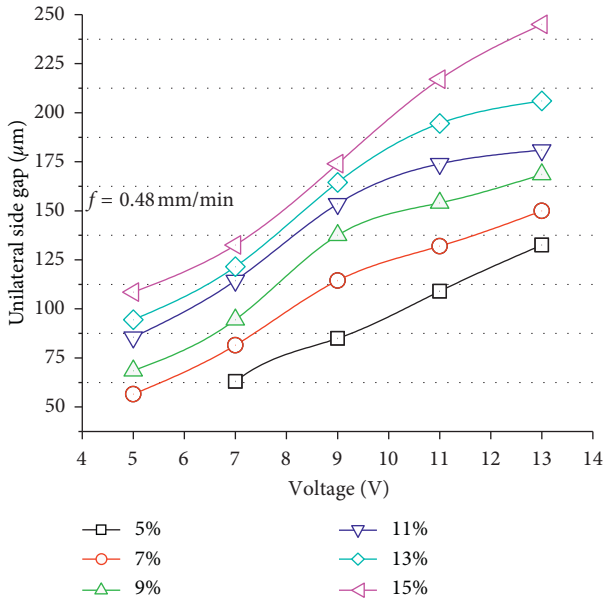

Figure 4: Variation curves of the unilateral side gap with the voltage.

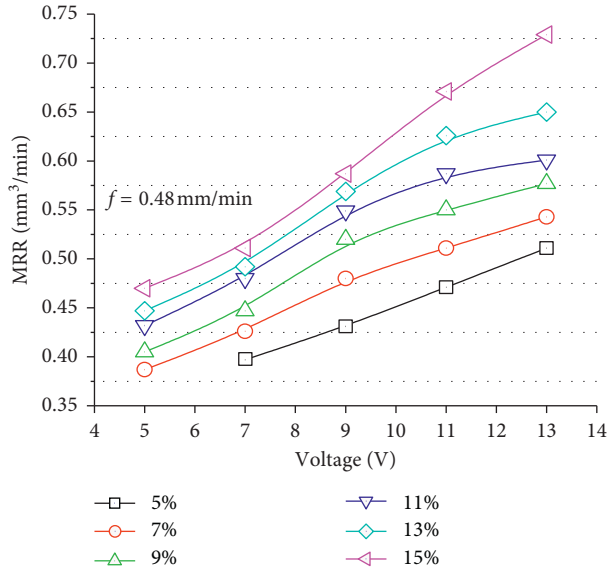

Figure 5: Variation curves of MRR with the voltage.

concentration is the same. At the electrolyte concentration of 13%, MRR increases by more than 45.4% (from 0.447 mm/min to 0.650 mm/min) as the applied voltage increases from 5 V to 13 V. Under the condition of other ECM parameters unchanged, higher applied voltage means more metal materials were dissolved from cooling hole per unit time.

Figure 6 shows three cooling hole samples machined by different applied voltages. The cooling hole shown in Figure 6(a) was machined at an electrolyte concentration of 5% and applied voltage of 5 V. Under these conditions, the ECM process stability cannot be guaranteed because the short circuit occurred contentiously and finally formed a "Blind Hole." The reason could be attributed to the fact that lower applied voltage and electrolyte concentration cannot provide strong material dissolution ability. Figure 6(b) shows an acceptable cooling hole shape, but there are also a small amount of edge corrosion around cooling hole edge with the occurrence of only one short circuit. In comparison, Figure 6(c) provides the best cooling hole forming without short circuits. Therefore, the increase of applied voltage can significantly improve process efficiency, accuracy, and stability for cooling hole making.

3.3. Effects of Electrolyte Concentration on Machining Accuracy and Efficiency. The electrolyte concentrations used in experiments for cooling hole making are 5%, 7%, 9%, 11%, 13%, and 15%. The electrode feed rate is also 0.48 mm/min. Figures 7 and 8 show the variation curves of the unilateral side gap Δs and MRR with the electrolyte concentration ξ.

Similar to Figure 4, the unilateral side gap Δs increases with the increasing of electrolyte concentration at all five certain applied voltages. For instant, at the applied voltage of 9 V, the unilateral side gap Δs increased by more than 120.4% (from 81 μm to 178.5 μm) as the electrolyte concentration increases from 5% to 13% (as shown in Figure 7). At the same time, MRR increases from 0.425 mm^3/min to 0.595 mm^3/min, increased by 40% (as shown in Figure 8). This could be explained as follows: higher electrolyte concentration means there exist more free moving ions in $NaNO_3$ solution, which could provide stronger current carrying capacity and enhance conductivity. In the EMC process for cooling hole making, higher electrolyte concentration leads to greater current density, and the metal material dissolution rate can be accelerated. Thus, Δs and MRR increase simultaneously as the electrolyte concentration increases.

Figure 9 shows three sample's morphology photos of cooling holes formed by different electrolyte concentrations (applied voltage $U = 15$ V). Under the electrolyte concentration of 7%, short circuits were detected 3 times and the hole roundness were relatively poor. In addition, serious corrosion occurs around the cooling hole edges (as shown in Figure 9(a)). The hole shown in Figure 9(b) only had a short circuit during machining, and the roundness and edge quality were improved. By contrast, the cooling hole in Figure 9(c) machined at the electrolyte concentration $\xi = 15\%$ possesses the best shape accuracy without short circuits. Therefore, the increase of electrolyte concentration can significantly improve the process efficiency, accuracy, and stability for cooling hole making, which is similar to applied voltage.

4. CFD Analysis of Electrolyte Flow Field

According to fundamental theories of ECM, the electrolyte flow status can significantly impact the discharge of electrochemical products and further impact the machining accuracy and efficiency in the cooling hole making process. In addition, existence of eddies may reduce the electrolyte flow velocity and decrease the stability of ECM. Unfortunately, the electrolyte flow status and eddy distributions

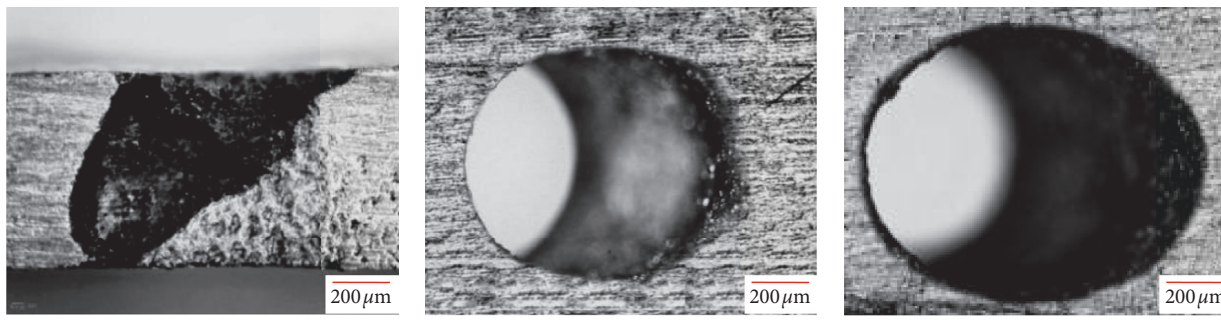

(a) (b) (c)

Figure 6: Cooling hole samples machined under different applied voltages. (a) $U = 5$ V, $\xi = 5\%$ (wt.%). (b) $U = 9$ V, $\xi = 5\%$ (wt.%). (c) $U = 13$ V, $\xi = 5\%$ (wt.%).

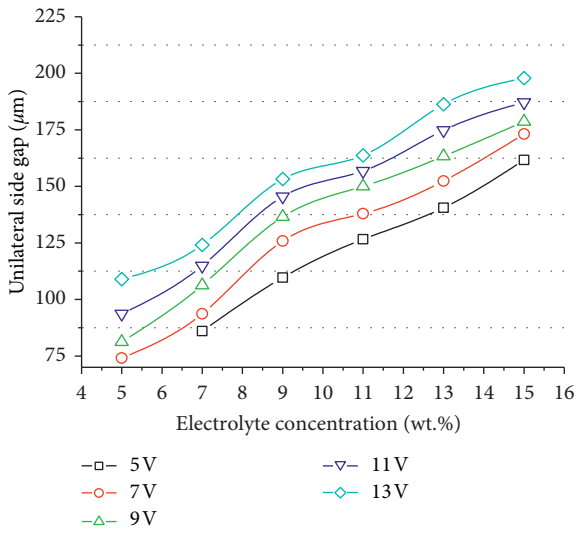

Figure 7: Variation curves of the unilateral side gap Δs with electrolyte concentration.

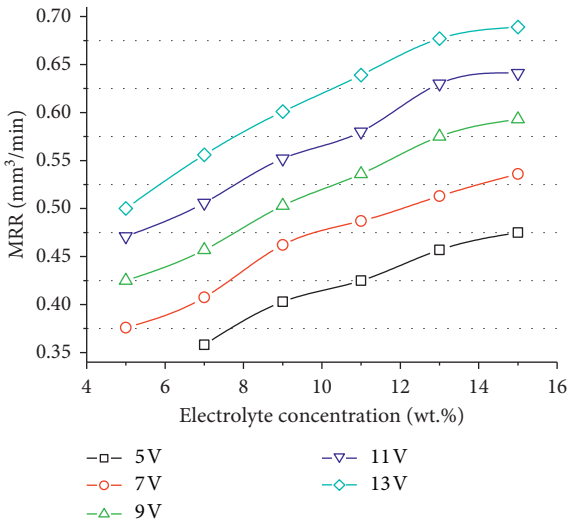

Figure 8: Variation curves of MRR with electrolyte concentration.

in the ECM process cannot be observed and recorded directly. Therefore, a simulation study becomes a feasible choice in ECM.

4.1. CFD Mode Building. Figure 10 is the schematic diagram of electrolyte fluid where a hole is being drilled by STEM. In the STEM process, the electrolyte flow field can be approximately divided into two areas, bottom flow area and side flow area. The flow field region is composed of the tool cathode contour, workpiece contour, and interelectrode gap. In order to obtain the necessary geometric information data for building CFD analysis CAD mode, all machined cooling hole samples were measured at five certain cross sections (as shown in Figure 11). Firstly, geometric data of Sections 1 and 5 can be measured directly. Subsequently, the samples were milled 3 times by using DMU 70 eVolution NC machine tools with the same milling depth 0.425 mm, and the geometric data of Sections 2, 3, and 4 can be measured and collected (as shown in Figure 12). Based on the measured 5 section geometric data, the CAD modes of the cooling hole were rebuilt by using UG software, and a typical CFD analysis mode is shown in Figure 13.

4.2. Effects of Applied Voltage and Electrolyte Concentration on Electrolyte Flow Velocity. In this study, six cooling hole samples were selected as the objective for CFD analysis. Three samples were machined under different applied voltages of 7 V, 9 V, and 13 V with unchanged electrolyte concentration $\xi = 9\%$ (experiment nos. 9, 15, and 27 listed in Table 2), and the other three samples were formed under different electrolyte concentrations of 7%, 11%, and 15% (wt.%) with the same applied voltage of 9 V (experiment nos. 14, 16, and 18 listed in Table 2).

In Figure 14, the unilateral side gap Δs and the bottom gap Δb increase with the increasing of applied voltage at the electrolyte concentration of 9%. The electrolyte flow velocity in the tube electrode inner hole also increases with the increase in applied voltage (the velocity field changes from green to yellow and then to orange). In the bottom gap area, all the maximum electrolyte flow velocities are approximately 30 m/s under different applied voltages of 7 V, 9 V, and 13 V. However, the unilateral gap side Δs and the bottom gap formed at the applied voltage of 13 V are obviously larger than those of 7 V and 9 V, which means more electrochemical products could be carried out in ECM area in unit time and consequently increase the MRR.

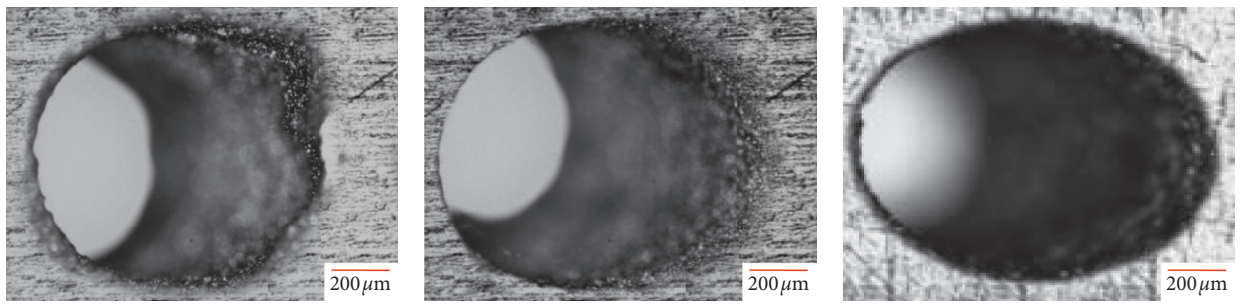

(a) (b) (c)

Figure 9: Cooling hole samples machined under different electrolyte concentrations. (a) $U = 15$ V, $\xi = 7\%$ (wt.%). (b) $U = 15$ V, $\xi = 11\%$ (wt.%). (c) $U = 15$ V, $\xi = 15\%$ (wt.%).

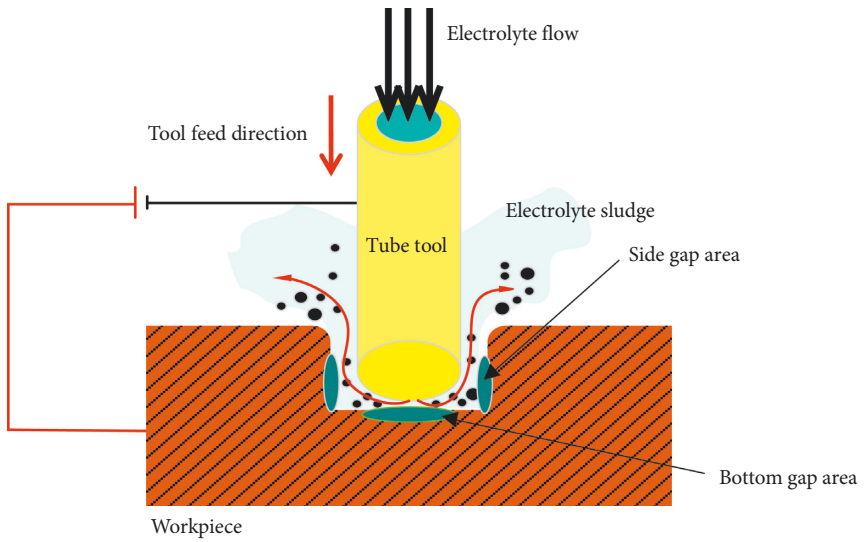

Figure 10: The schematic diagram of electrolyte fluid.

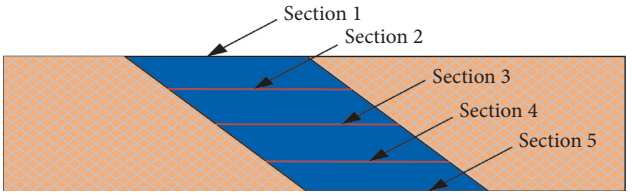

Figure 11: Measured sections of the cooling holes sample.

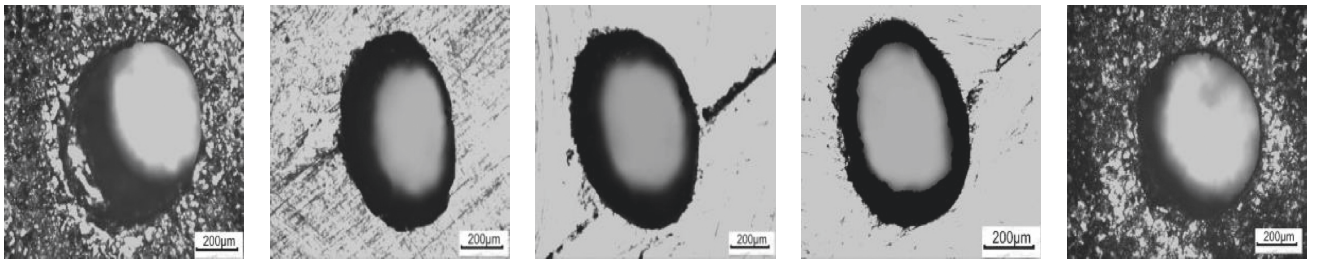

(a) (b) (c) (d) (e)

Figure 12: Milled sections of a machined cooling hole samples. (a) Section 1. (b) Section 2. (c) Section 3. (d) Section 4. (e) Section 5.

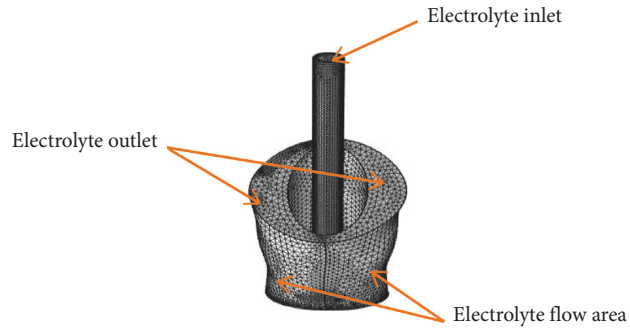

Figure 13: CFD analysis mode of cooling hole (electrolyte encapsulation area).

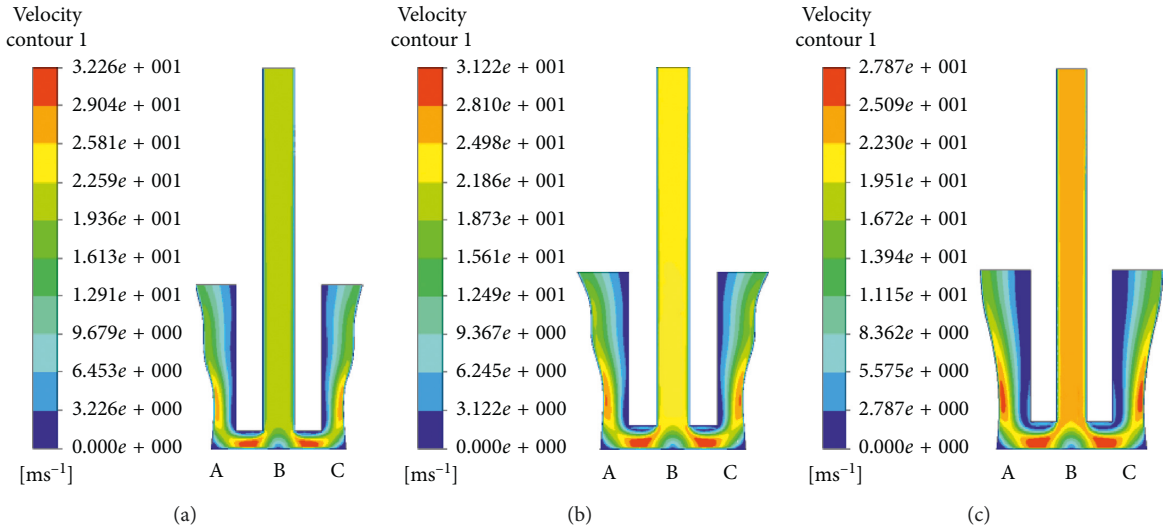

Figure 14: Electrolyte flow velocity distribution under different applied voltages. (a) $U = 7$ V, $\xi = 9\%$ (wt.%). (b) $U = 9$ V, $\xi = 9\%$ (wt.%). (c) $U = 13$ V, $\xi = 9\%$ (wt.%).

Similar to Figure 14, in the case of other ECM process parameters unchanged, the electrolyte flow velocity in the tube electrode inner hole increases with the electrolyte concentration increase (from 24.85 m/s to 28.35 m/s), which means that the electrolyte pump needs to provide more electrolyte solution in unit time. In addition, size of the unilateral side gap Δs and the bottom gap Δb also becomes larger with increase in electrolyte concentration. In the bottom gap area, the high-velocity flow region of an electrolyte (red color region) is enlarged with electrolyte concentration ξ variation from 7% to 15%. The same variation tendency may be observed in the side gap (Figures 15(a)–15(c)). A larger machining gap, more electrolyte supply, and higher flow velocity of electrolyte make it easier to discharge electrochemical products and further improve MRR.

4.3. Effects of Applied Voltage and Electrolyte Concentration on Electrolyte Flow Eddy. In this study, the influence of applied voltage and electrolyte concentration on electrolyte flow eddy distribution was analyzed by simulating the cooling hole samples selected (see Section 4.2).

Figures 16(a)–16(c) shows us the distribution status of electrolyte flow eddies with applied voltage variation at unchanged electrolyte concentration $\xi = 9\%$. It is obvious that the eddies are mainly locate in the bottom gap area. With the increase in applied voltage, the eddy current area becomes larger, but the turbulent kinetic energy exhibits decreased tendency. For instance, at the electrolyte concentration of 9%, the turbulent kinetic energy decreases by more than 34.49% (from 79.32 J/kg to 51.96 J/kg) as the applied voltage increases from 7 V to 13 V. Higher turbulent kinetic energy means more serious eddy current, which could result in metal dissolved products staying in the bottom gap area, consequently increasing short circuit probability. According to experiment records, at the applied voltage of 13 V and electrolyte concentration of 9%, the cooling holes were machined successfully without the occurrence of short circuits. In comparison, four times and one time short circuits were detected at the applied voltage of 7 V and 9 V, respectively. Therefore, ECM process stability may be improved in the case of lower eddy current energy. In addition, there are some lower intensity eddies locating in the side gap area. Because the outer wall of the tube electrode

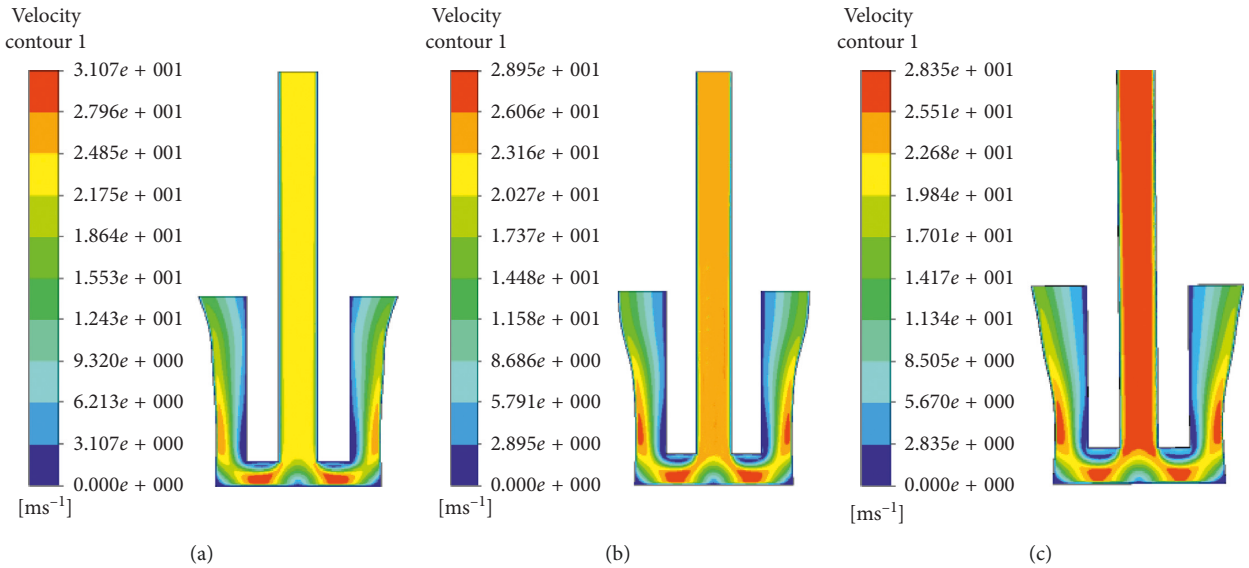

FIGURE 15: Electrolyte flow velocity distribution under different electrolyte concentrations. (a) $U = 9$ V $\xi = 7\%$ (wt.%). (b) $U = 9$ V $\xi = 11\%$ (wt.%). (c) $U = 9$ V $\xi = 15\%$ (wt.%).

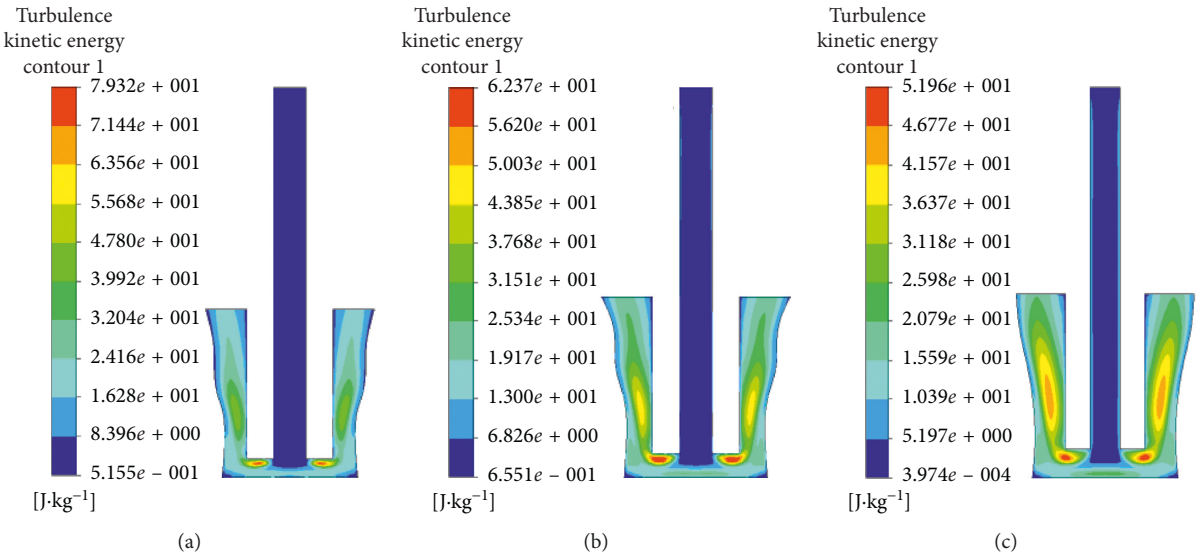

FIGURE 16: Electrolyte flow eddy distribution under different applied voltages. (a) $U = 7$ V, $\xi = 9\%$ (wt.%). (b) $U = 9$ V, $\xi = 9\%$ (wt.%). (c) $U = 13$ V, $\xi = 9\%$ (wt.%).

was insulated, there is no electric field in the side gap zone. Therefore, metal dissolution does not occur in this specialized zone. The harmful effects of low-intensity eddies on ECM process stability in the side gap area may be ignored nearly.

Figure 17 shows us the distribution status of electrolyte flow eddies with electrolyte concentration variation at unchanged applied voltage. In Figures 17(a)–17(c), two key points needs special attention. On one hand, with the electrolyte concentration increase, the turbulence kinetic energy decreases gradually. At the applied voltage of 9 V, the turbulent kinetic energy of eddy decreases by more than 29.88% (from 64.79 J/kg to 45.43 J/kg) as the electrolyte concentration increases from 7% to 15%. On the other hand, the eddies show an exciting trend to leave the bottom gap and then enter the side gap region in the case of increase in electrolyte concentration. Compared with high-intensity eddies, low-intensity eddies cannot cause serious accumulation of electrochemical products. The eddies entering the side gap region would be favorable to dissolve the metal materials at the bottom of cooling holes smoothly. In addition, the outer wall of the tube electrode was insulated, and the eddies may have no harmful effects on the shape accuracy of the machined cooling hole. Consequently, the portability of short circuit occurrence will reduce. For instance, two times short circuits were detected at the

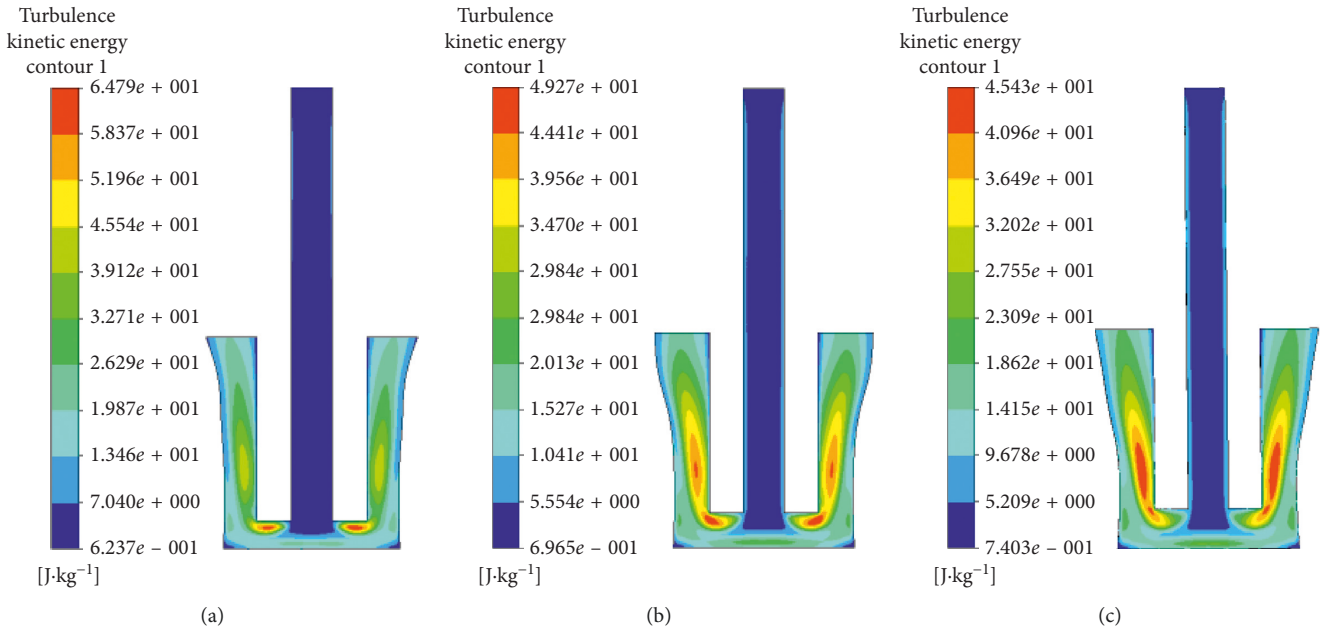

FIGURE 17: Electrolyte flow eddy distribution under different electrolyte concentrations. (a) $U = 9$ V, $\xi = 7\%$. (b) $U = 9$ V, $\xi = 11\%$. (c) $U = 9$ V, $\xi = 15\%$.

electrolyte concentration of 7% and no short circuit was detected at the electrolyte concentration of 11% and 15%.

5. Conclusions

In this paper, the influence of applied voltage and electrolyte concentration on process efficiency, form accuracy, and stability of cooling hole making in STEM were investigated by means of full factorial design of experiments. Moreover, the electrolyte flow velocity field and eddy distribution status were evaluated and determined by CFD simulation analysis, which possess guiding significance for the optimization of process parameters of ECM. Key findings are as follows:

(i) The unilateral side gap Δs and MRR increase obviously with the increase of applied voltage and electrolyte concentration. The shape accuracy of cooling holes including hole roundness and edge quality was improved with the increasing of applied voltage and electrolyte concentration.

(ii) Higher process stability may be obtained in the case of higher applied voltage and electrolyte concentration because the relatively large side gap Δs and the bottom gap Δb could provide stronger discharge capacity of electrolytic products and reduce short circuit portability.

(iii) With the increase of applied voltage and electrolyte concentration, the flow velocity of electrolyte solution becomes faster, but the turbulence kinetic energy of eddy decreased. In addition, the eddy distribution shows the tendency to leave the bottom gap and enter the side gap with the increase in electrolyte concentration, which will be beneficial to improve ECM process stability for cooling hole making.

Data Availability

The prior studies and datasets are cited at relevant places within the text as references [15–17].

Conflicts of Interest

The authors declare that they have no conflicts of interest.

Acknowledgments

This project was supported by the Natural Science Foundation of China (No. 51775321).

References

[1] S. Peetermans and E. H. Lehmann, "Simultaneous neutron transmission and diffraction imaging investigations of single crystal nickel-based superalloy turbine blades," *NDT & E International*, vol. 79, pp. 109–113, 2016.

[2] D. Liu, J. Jin, Y. Peng, and X. Hu, "Summarization of development status and key technologies for large airplane engines," *Journal of Aerospace Power*, vol. 23, no. 6, pp. 976–980, 2008.

[3] D. S. Bilgi, V. K. Jain, R. Shekhar, and S. Mehrotra, "Electrochemical deep hole drilling in super alloy for turbine application," *Journal of Materials Processing Technology*, vol. 149, no. 1–3, pp. 445–452, 2004.

[4] X. Liu, C. Tao, C. Liu, C. Hu, and X. Chen, "Investigation of processing methods and development of gas holes of engine blade," *Materials Review*, vol. 27, no. 11, pp. 117–120, 2013.

[5] F. Wang, *Test and Technology Research on Electrochemical and Discharge Hybrid Machining for Micro Hole of Difficult-to-Machining Material*, Nanjing University of Aeronautics and Astronautics, Nanjing, China, 2017.

[6] Y. Zhang, N. Qu, X. Fang, and X. Wang, "Eliminating spikes by optimizing machining parameters in electrochemical drilling," *Journal of Manufacturing Processes*, vol. 37, pp. 488–495, 2019.

[7] V. K. Jain and P. C. Pandey, "Investigations into the use of bit as a cathode in ECM," *International Journal of Machine Tool Design and Research*, vol. 22, no. 4, pp. 341–352, 1982.

[8] S. Ali, S. Hinduja, J. Atkinson, and M. Pandya, "Shaped tube electrochemical drilling of good quality holes," *CIRP Annals*, vol. 58, no. 1, pp. 185–188, 2009.

[9] X. Chen, Z. Xu, D. Zhu, Z. Fang, and D. Zhu, "Experimental research on electrochemical machining of titanium alloy Ti60 for a blisk," *Chinese Journal of Aeronautics*, vol. 29, no. 1, pp. 274–282, 2016.

[10] W. Wang, D. Zhu, N. Qu, S. Huang, and X. Fang, "Electrochemical drilling inclined holes using wedged electrodes," *The International Journal of Advanced Manufacturing Technology*, vol. 47, no. 9–12, pp. 1129–1136, 2010.

[11] Z. Y. Li, X. T. Wei, J. J. Sun, C. W. Zang, C. H. Fu, and Y. B. Guo, "Process capability and effect size of vacuum extraction shaped tube electrolytic drilling of Inconel alloy for high-performance cooling hole," *The International Journal of Advanced Manufacturing Technology*, vol. 85, no. 9–12, pp. 2557–2566, 2016.

[12] S. R. Rao, G. Padmanabhan, K. M. Naidu, and A. Rukesh Reddy, "Parametric study for radial over cut in electrochemical drilling of Al-5%B_4C_p composites," *Procedia Engineering*, vol. 97, pp. 1004–1011, 2014.

[13] C. Gao, N. Qu, H. He, and L. Meng, "Double-pulsed wire electrochemical micro-machining of type-304 stainless steel," *Journal of Materials Processing Technology*, vol. 266, pp. 381–387, 2019.

[14] K. P. Rajurkar, M. M. Sundaram, and A. P. Malshe, "Review of electrochemical and electrodischarge machining," *Procedia CIRP*, vol. 6, pp. 13–26, 2013.

[15] D. S. Bilgi, V. K. Jain, R. Shekhar, and A. V. Kukarni, "Hole quality and interelectrode gap dynamics during pulse current electrochemical deep hole drilling," *The International Journal of Advanced Manufacturing Technology*, vol. 34, no. 1-2, pp. 79–95, 2007.

[16] D. S. Bilgi, R. Kumar, V. K. Jain, and R. Shekhar, "Predicting radial overcut in deep holes drilled by shaped tube electrochemical machining," *The International Journal of Advanced Manufacturing Technology*, vol. 39, no. l-2, pp. 47–54, 2008.

[17] X. Hu, D. Zhu, J. Li, and Z. Gu, "Flow field research on electrochemical machining with gas film insulation," *Journal of Materials Processing Technology*, vol. 267, pp. 247–256, 2019.

[18] R. Wu, J. Xu, and J. Zhao, "Fluid field simulation of electrochemical machining cavities based on software of CFD," *China Mechanical Engineering*, vol. 19, no. 14, pp. 1657–1660, 2008.

[19] D. Zhu, Z. Gu, T. Xue, and A. Liu, "Simulation and experimental investigation on a dynamic lateral flow mode in trepanning electrochemical machining," *Chinese Journal of Aeronautics*, vol. 30, no. 4, pp. 1624–1630, 2017.

[20] W. Wang, D. Zhu, N. S. Qu, S. F. Huang, and X. L. Fang, "Electrochemical drilling with vacuum extraction of electrolyte," *Journal of Materials Processing Technology*, vol. 210, no. 2, pp. 238–244, 2010.

[21] D. Zhu, W. Wang, X. L. Fang, N. S. Qu, and Z. Y. Xu, "Electrochemical drilling of multiple holes with electrolyte-extraction," *CIRP Annals*, vol. 59, no. 1, pp. 239–242, 2010.

[22] S. Wei, Z. Xu, L. Sun, D. Zhu, and D. Zhu, "Analysis on forming laws of blisk tunnel in radial feed electrochemical machining and cathode design," *Electromachining & Mould*, vol. 3, pp. 36–40, 2012.